



Indandione oligomer@graphene oxide functionalized nanocomposites for enhanced and selective detection of trace Cr²⁺ and Cu²⁺ ions

Eun-Bi Kim^{1,2} · M. Imran² · Ahmad Umar³ · M. Shaheer Akhtar⁴ · Sadia Ameen²

Received: 15 October 2021 / Revised: 17 January 2022 / Accepted: 22 January 2022 / Published online: 15 February 2022
© The Author(s), under exclusive licence to Springer Nature Switzerland AG 2022

Abstract

Herein, using 1, 3 indandione and three thiophene unit by Suzuki coupling reaction, small organic oligomer-based indandione derivative, 2-(5''-hexyl-[2,2':5'2'' terthiophen]-5-yl) methylene)-1H-indene-1,3(2H) dione oligomer (HTD) was synthesized. A functional and highly effective nanocomposite based on the synthesized HTD oligomer and graphene oxide (GO) was further synthesized and utilized to fabricate high-sensitive and selective chemical sensor. The synthesized HTD@GO functionalized nanocomposites were further examined by several techniques and finally coated on the glassy carbon electrode (GCE) to fabricate the chemical sensor. Due to the synergistic impacts of HTD oligomer and GO, the functionalized HTD@GO nanocomposite exhibited outstanding physiochemical, structural, and surface characteristics. Thus, using an electrochemical method, the HTD@GO/GCE sensor probe demonstrated the outstanding simultaneous trace detection of heavy metals such as Cr²⁺ and Cu²⁺ ions. The HTD@GO/GCE sensor probe revealed a strong selectivity towards Cr²⁺ and Cu²⁺ ions when compared to other metal ions (Al³⁺, Zn²⁺, K⁺, Mn²⁺). Importantly, the HTD@GO/GCE-based sensor exhibited relatively good dynamic linear ranges of 1–100 μM and detection limit values of ~3.65 μM and ~2.25 μM, respectively, for trace Cr²⁺ and Cu²⁺ ions. The HTD@GO/GCE sensor probe has low relative standard deviations (RSDs) of ~10% and ~6.4% for Cr²⁺ and Cu²⁺ ions, respectively, as suggested by the repeatability test. Analyzing actual water samples was also used to test the reliability of the functionalized nanocomposite sensor.

Keywords Indandione oligomer · Graphene oxide · Electrode · Electrochemical properties · Heavy metal detection

1 Introduction

Organic semiconducting or electronic materials remain of vital interest in the field of electrochemistry for their flexibility in chemical and electrochemical behavior. Electrochemical sensors are becoming popular, owing to their good detection performances, ease of operation, less expensive, fast, and selective analytic technique [1]. The sensing performance is highly influenced by the electrode materials for enhancing the catalytic effects and elimination of interferers; thus, it is of great importance to design new electrode materials. For developing electrode materials, we can hardly ignore conjugated organic semiconductors due to their high electrical conductivity, highly efficient, tailorable charge transport characteristics, and rapid signal transduction [2–6]. Due to associate π-conjugation in the backbone of conjugated organic semiconductors [7, 8], they exhibit a direct interaction with the analyte in a redox process and thus, help in increasing the selectivity and sensitivity. Park et al.

✉ M. Shaheer Akhtar
shaheerakhtar@jbnu.ac.kr

✉ Sadia Ameen
sadiaameen@jbnu.ac.kr

¹ School of Chemical Engineering, Jeonbuk National University, Jeonju 54896, Republic of Korea

² Advanced Materials and Devices Laboratory, Department of Bio-Convergence Science, Jeonbuk National University, Jeongeup Campus 56212, Republic of Korea

³ Department of Chemistry, Faculty of Science and Arts and Promising Centre for Sensors and Electronic Devices (PCSED), Najran University, Najran 11001, Saudi Arabia

⁴ New & Renewable Energy Material Development Center (NewREC), Jeonbuk National University, Jeonbuk, Republic of Korea

fabricated chromium (VI) sensor based on catalytic reduction using the nanoporous layer of poly (aminopyrimidyl-terthiophene)/AuNi composite and reported the detection limit of 0.25 ± 0.05 ppb [9]. Shim and co-workers developed chronocoulometric sensor for heavy metal ions using a diaminoterthiophene modified electrode doped with graphene oxide [10]. In another report, Lee and his research group compared enzymatic and non-enzymatic glucose sensors based on hierarchical Au-Ni alloy with conductive polymer. The linear range of enzymatic sensor was attained from 1 μM –30 mM with a detection limit of 0.29 μM [11]. In search of important findings related to conjugated organic semiconductors, this work reports the synthesis of indandione oligomer as electrode material. Our synthetic strategy is to design a small molecule semiconductor, 2-(5''-hexyl-[2,2':5'2'' terthiophen]-5-yl) methylene)-1H-indene-1,3(2H) dione, HTD, comprised of 1, 3 indandione and three thiophene (3 T) unit containing one hexyl side chain. In synthesized HTD, hexyl side chain not only enhances the solubility in common organic solvents but also helpful for molecular packing, improves the charge transport properties, and supports the formation of excellent thin films [12].

Rapid industrialization has led to the release of heavy metals ions such as Cd^{2+} , Pb^{2+} , and Cu^{2+} ions in wastewater. These highly toxic and non-degradable heavy metals are not only imposing threats to the environment but also destructing the health of living beings [13–16]. The intake of heavy metal by the human body, even at trace concentrations, might cause irreversible damage to human health [17–20]. Averting the harm of heavy metal ions to the environment and humans, it is quite demanding to develop a direct and highly sensitive determination method in monitoring the contamination. Among the detection methods, conventional analytical techniques such as atomic absorption spectroscopy (AAS), inductively coupled plasma atomic emission spectroscopy (ICP-AES), inductively coupled plasma mass spectrometry (ICP-MS), and hyper-Rayleigh scattering, fluorescence detection [21, 22] are largely explored but despite of exhibiting high sensitivity and reproducibility; the implementation of these techniques is expensive which restricts their usage [23]. Moreover, most of the determination methods are focused on single ion detection, and thus, simultaneous detection of heavy metal ions is challenging due to mutual interference between heavy metal ions, the formation of intermediate alloys, and competitive adsorption on active sites [24–26]. Currently, square wave anodic stripping voltammetry (SWASV), one of the electrochemical methods, displays impressive ability of simultaneous determination of trace heavy metal ions, shows excellent sensitivity, low detection limits, portable, and of cheap cost [27, 28]. Armstrong et al. developed bismuth-based electrode for the stripping analysis of heavy metal ions and obtained a high sensitivity with low detection limits of ~ 93 ng L^{-1}

and ~ 54 ng L^{-1} for Pb (II) and Cd (II), respectively [29]. Wang and co-workers established simultaneous detection of three main heavy metal ion pollutants (Cd^{2+} , Pb^{2+} , and Cu^{2+} ions) with improved reproducibility and reliability using SWASV method [30]. Simultaneous detection of Cd^{2+} , Cu^{2+} , Hg^{2+} , and Pb^{2+} ions with low detection limits and wide dynamic ranges was performed by differential pulse voltammetry (DPV) measurements [31]. Suvina et al. studied the formation of novel hydrogels of conjugate polymer polypyrrole (PPy) and reduced graphene oxide (rGO) for the simultaneous detection of four different heavy metals ions such as Cd^{2+} , Pb^{2+} , Cu^{2+} , and Hg^{2+} [32]. A variety of electrode surface modifications have been explored for increasing the sensing performances. One common approach of modifying the electrode surface is using graphene oxide (GO) due to the high specific surface area, chemical stability, high π -conjugation, and hydrophilic properties [33, 34]. The aim of this research work is the modification of GCE through the functionalization of indandione oligomer (HTD) with GO. The presence of π -bond in HTD oligomer supports the surface adsorption of GO due to π - π^* stacking interactions, hydrogen bond, and Vander Waals interactions [35]. Herein, the incorporation of carbonaceous material to HTD oligomer can improve the electroanalytical qualities of the system through an increase in the surface area and can improve the mass transport of the analyte. Moreover, the properties like electrical conductivity and dispensability are also improved due to the synergistic effect of HTD oligomer and GO. To the best of our knowledge, it is the first report of sensitive and selective simultaneous detection of Cr^{2+} and Cu^{2+} ions with HTD@GO/GCE sensor probe by a simple electrochemical method at room conditions.

2 Experimental section

2.1 Synthesis of 2-(5''-hexyl-[2,2':5'2'' terthiophen]-5-yl) methylene)-1H-indene-1,3(2H) dione (HTD)

HTD oligomer was synthesized by the simple coupling reaction using 1, 3 Indandione (**1**) and 2-(5-brmothiophen-2-yl) methylene)-1H-indene-1,3(2H)-dione (**2**) [36], as illustrated in scheme 1 (supporting information). The coupling reaction for HTD oligomer was obtained by mixing (**2**) (0.35 g, 1.09 mmol), 2-(5'-hexyl-[2, 2'-bithiophen]-5-yl)-4, 4, 5, 5-tetramethyl-1, 3, 2-dioxaborolane (0.53 g, 1.42 mmol), and 5 mol % $\text{Pd}(\text{PPh}_3)_4$ in anhydrous toluene (C_7H_8 , 20 ml, Sigma Aldrich) and stirred in a round bottom flask. After that, potassium carbonate (K_2CO_3 , 2 M, Sigma Aldrich) in 5 ml of deionized (DI) water was introduced into the reaction mixture, and refluxed at 110 °C for 24 h under argon

atmosphere. After completion, the cooled reaction mixture was quenched with DI water, and sequential washing with brine and DI was performed. An organic phase was then extracted with dichloromethane (DCM) and dried over magnesium sulfate (MgSO_4 , Sigma Aldrich). The resultant solution was filtered, evaporated in vacuum under reduced pressure and the obtained residue was further purified by flash column using (dichloromethane (DCM): heaxane (C_6H_{14}), 1:4 v/v) and recrystallized (DCM: EtOH, 1: 5 v/v) (yield 67.62% 0.36 g). ^1H NMR (500 MHz, CDCl_3 , ppm) δ : 7.91 (m, 2H), 7.85 (s, 1H), 7.80 (d, $J=4.1$ Hz, 2H), 7.73 (m, 2H), 7.32 (d, $J=3.9$ Hz, 1H), 7.20 (d, $J=4.0$ Hz, 1H), 7.04–7.09 (dd, $J=4.1$ Hz, 3.7 Hz 2H), 6.68 (d, $J=3.6$ Hz, 1H), 2.78 (t, $J=7.5$ Hz, 2H), 1.65 (m, 4H), 1.34 (m, 4H), 0.89 (t, $J=6.9$ Hz, 3H). ^{13}C NMR (100 MHz, CDCl_3 , ppm) δ : 190.42, 189.82, 150.36, 146.92, 143.81, 142.04, 140.54, 140.41, 135.93, 135.83, 135.01, 134.80, 134.24, 133.98, 127.35, 125.22, 124.52, 124.40, 124.16, 123.46, 122.99, 122.82, 31.65, 31.60, 30.32, 28.85, 22.67, 14.18. MS: m/z calc. for $[\text{C}_{28}\text{H}_{24}\text{O}_2\text{S}_3 + \text{H}]^+$: 489.68; found: 489.56.

2.2 Fabrication of sensor probe

GO was prepared according to modified Hummer's method using the graphite powder [37]. Optimized solution of HTD oligomer (10 mg) with different amounts of GO (0.2 mg, 0.5 mg and 1 mg) were dispersed in 1 ml chlorobenzene solvent and drop casted on cleaned GCE, followed by drying in air oven at 70 °C. Herein, prior to the deposition, GCE was cleaned by using wet soft polishing cloth with alumina powder (0.5 and 0.03 μm , successively), followed by cleaning with DI water and ethanol. Synthesized HTD@GO functionalized nanocomposite was used as sensor probe for the simultaneous detection of Cr^{2+} and Cu^{2+} ions.

2.3 Characterizations of HTD oligomer and HTD@GO functionalized nanocomposite

The configuration and structure of HTD oligomer were confirmed by nuclear magnetic resonance spectroscopy with (^1H NMR, JEOL FT-NMR) in deuterated chloroform

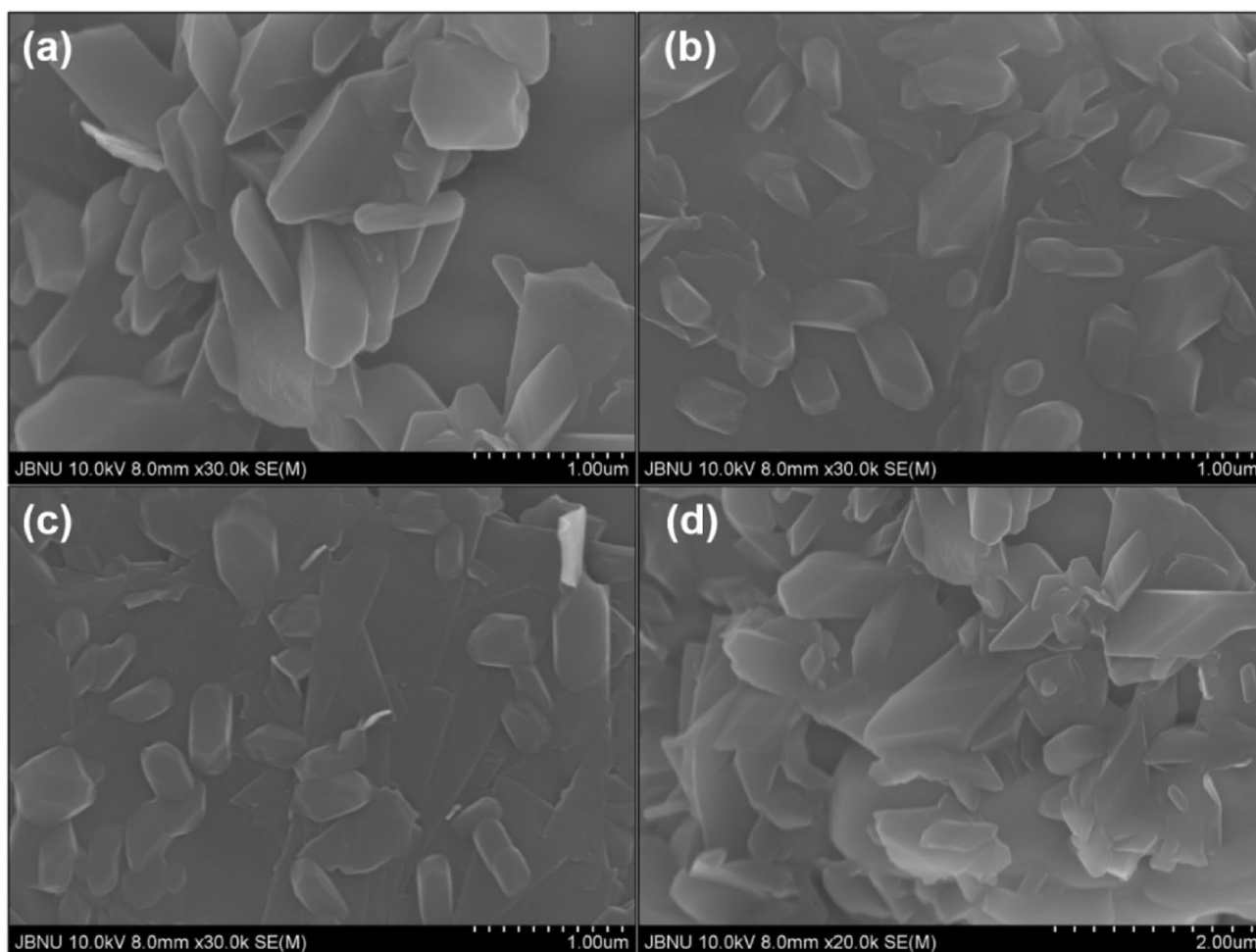


Fig. 1 FESEM images of **a** HTD oligomer and HTD@GO functionalized nanocomposite with **b** 0.2 mg GO, **c** 0.5 mg GO, and **d** 1 mg GO

(CDCl₃) solvent at 600 MHz for ¹H and 100 MHz for ¹³C13. High-resolution mass spectrometry was used to support the synthesis of HTD oligomer. The presence of bond structures was examined by Fourier transform infra-red spectroscopy by using JASCO FTIR-4100 Japan. The morphological observations of as-synthesized HTD@GO functionalized nanocomposite were observed by field emission scanning electron microscope (FESEM, Hitachi S-4700). The absorption and photoluminescence (PL) spectrum of HTD@GO functionalized nanocomposite were recorded by UV–Visible spectrophotometer (JASCO, V-670) and FP-6500 (JASCO) respectively. The structural modifications of HTD@GO functionalized nanocomposite were studied by Raman scattering (Raman microscope, Renishaw). X-rays photoelectron spectroscopy (XPS) was performed by using AXIS-NOVA CJ109, Kratos Inc., ranges 0–800 eV for surface composition and the surface interaction of HTD@GO functionalized nanocomposite. The cyclic voltammetry (CV) experiments

were conducted in 0.1 M phosphate buffer solution (PBS, pH=7) at the scan rate of 50 V/s, using WPG100 electrochemical measurement system which was carried out using 10 ml electrochemical cell comprising of three-electrode system including GCE working electrode, Pt wire as counter electrode and Ag/AgCl reference electrode.

3 Results and discussion

3.1 Formation and morphological studies of HTD@GO functionalized nanocomposite

The formation of HTD oligomer is confirmed by various spectroscopic characterizations such as ¹HNMR, ¹³CNMR, FTIR, and high resolution mass spectrometry (HRMS), as given in supporting information (SI). The morphologies of HTD oligomer and HTD@GO functionalized

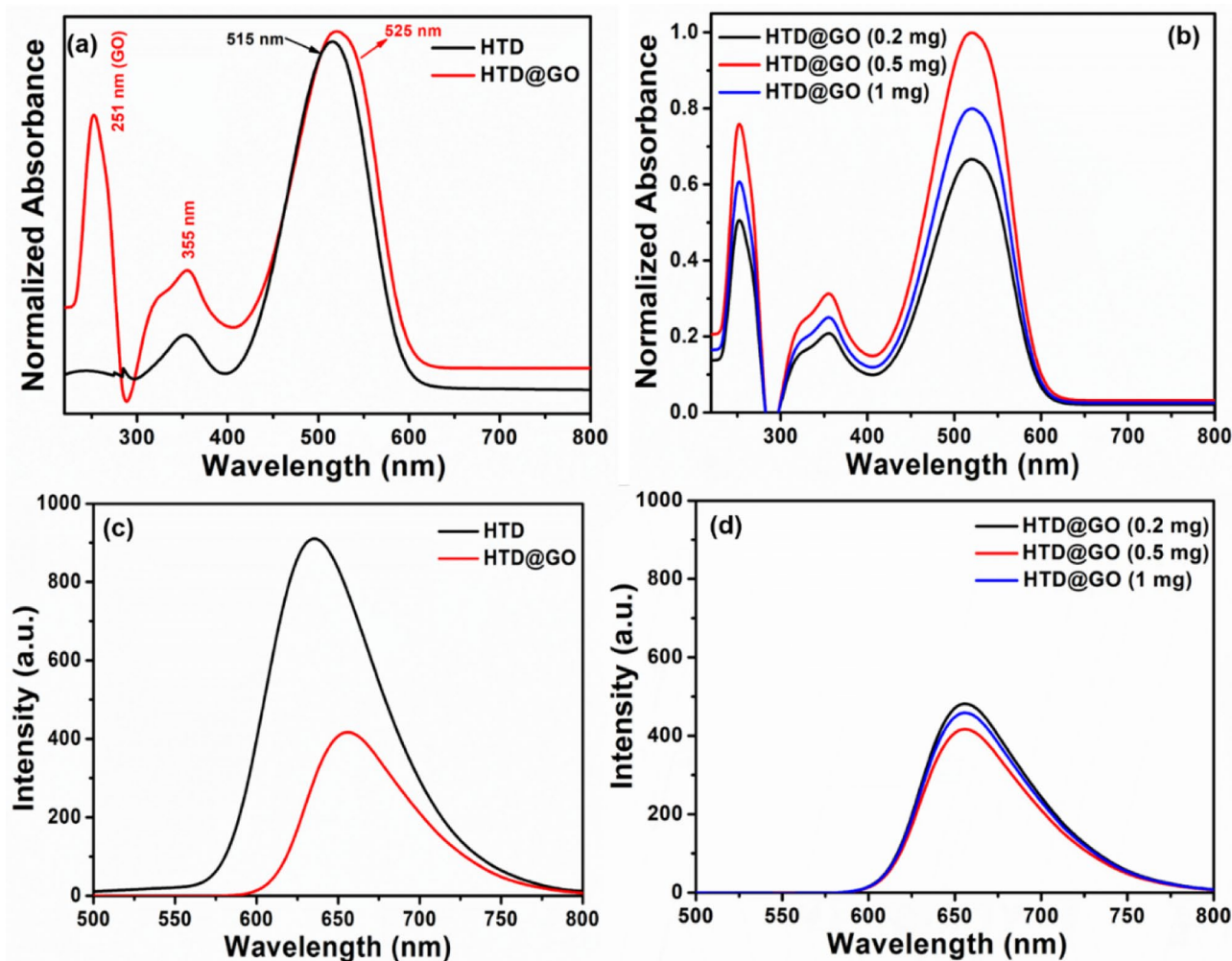


Fig. 2 UV–vis absorption spectra of **a** HTD oligomer, HTD@GO functionalized nanocomposite; **b** HTD@GO functionalized nanocomposite with various GO concentrations; **c** photoluminescence (PL)

spectra of HTD oligomer, HTD@GO functionalized nanocomposite; and **d** HTD@GO functionalized nanocomposite with various GO concentrations

nanocomposite are investigated by FESEM analysis. Figure 1a shows irregular small rods like morphology of HTD oligomer which is the usual morphology of organic small molecule [38]. From Fig. 1b, c, HTD@GO functionalized nanocomposites show uniformly mixed morphology of HTD oligomer and GO. Moreover, a high amount of GO (1 mg) in HTD@GO functionalized nanocomposite, as depicted in Fig. 1d, causes an agglomeration of rods and GO which results in large aggregates. Thus, GO (0.5 mg) in HTD@GO nanocomposite is the optimized ratio for obtaining the uniform and well-mixed thin film. Herein, HTD oligomer might form the bond with GO, which will be later confirmed by XPS studies.

3.2 Optical properties of HTD@GO functionalized nanocomposite

UV–Vis absorption was recorded quantitatively in chloroform solution for HTD oligomer and HTD@GO functionalized nanocomposites. From Fig. 2a, the synthesized HTD oligomer presents an absorption band at ~ 355 nm, referring to π - π^* transition, whereas the dominant absorption band at ~ 515 nm indicates n - π^* transitions of HTD oligomer [39].

However, HTD@GO functionalized nanocomposite displays three absorption bands at ~ 251 nm, ~ 355 nm and ~ 525 nm, corresponding to the characteristics bands of GO and HTD oligomer, respectively [40]. Significantly for HTD@GO functionalized nanocomposite, a slight shift of absorption band towards a higher absorption edge indicates π - π^* interaction between HTD oligomer and GO [41]. From Fig. 2b, GO (0.5 mg) in HTD@GO functionalized nanocomposite shows the highest absorption intensity as compared to other ratio of HTD@GO functionalized nanocomposites, which again suggests a good mixing of

GO and HTD oligomer. Furthermore, PL spectra of HTD oligomer and HTD@GO functionalized nanocomposites are examined using an excitation wavelength of ~ 350 nm, as shown in Fig. 2c, d. HTD oligomer displays a prominent emission PL peak centered at ~ 635 nm in the green region due to the benzenoid groups of HTD oligomer [36]. Referring to HTD@GO functionalized nanocomposite, a considerable shift from 635 to ~ 656 nm with prominent PL quenching is observed. This quenching describes the generation of singlet excitons [42]. The quenching is intensified after an interaction of GO with HTD oligomer. HTD@GO functionalized nanocomposite with GO (0.5 mg) displays the maximum quenching, suggesting the emission process of conjugated organic semiconductors like HTD oligomer.

3.3 Structural characterization of HTD@GO functionalized nanocomposite

HTD oligomer and HTD@GO functionalized nanocomposite are further analyzed by FTIR spectra, as shown in Fig. 3a. Herein, HTD oligomer shows C-H stretching (aliphatic) at ~ 2922 and ~ 2861 cm^{-1} , C=O stretching at ~ 1716 and ~ 1672 cm^{-1} , C=C stretching is displayed at ~ 1576 cm^{-1} , and C=C (aromatic) stretching appears at ~ 1432 cm^{-1} , and H-C-H bonding are shown by the peaks at ~ 1380 and ~ 1337 cm^{-1} [43]. The other peak for C-S-C bending is visible at ~ 1196 cm^{-1} , and C-S stretching appears at ~ 97 and ~ 726 cm^{-1} [44]. However, in HTD@GO functionalized nanocomposite, IR bands are shifted negatively to ~ 1708 cm^{-1} , ~ 1568 cm^{-1} , and ~ 1231 cm^{-1} indicating the linkage between GO and HTD oligomer. Considerably, the marginal shifting in IR band at ~ 1568 cm^{-1} and ~ 1708 cm^{-1} again supports the interaction between GO and HTD

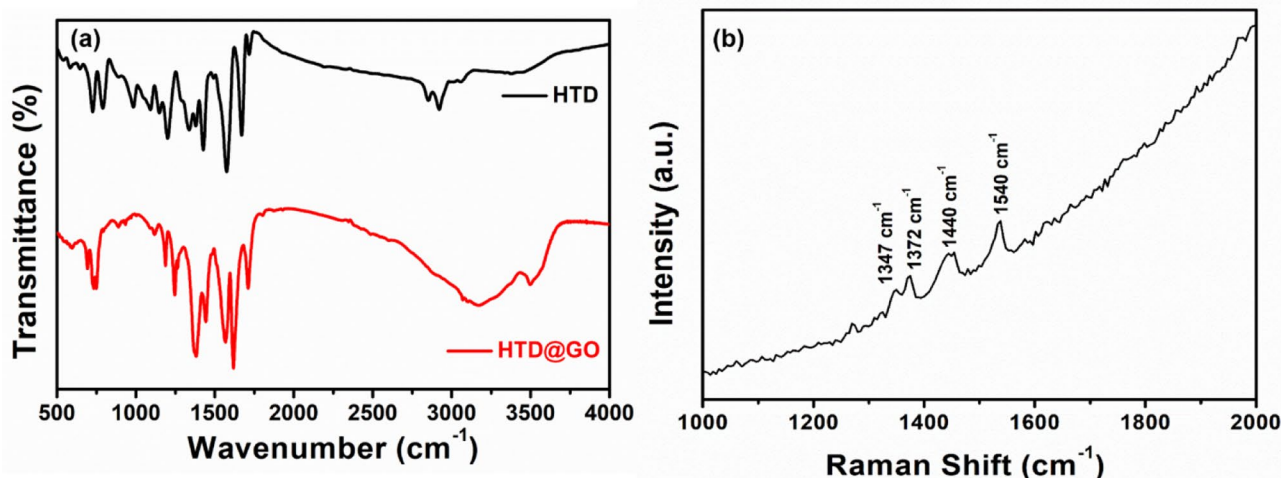


Fig. 3 **a** FTIR spectra of HTD oligomer, HTD@GO functionalized nanocomposite, and **b** Raman spectrum of HTD@GO functionalized nanocomposite with 0.5 mg GO

oligomer via π - π^* interactions and partial hydrogen bonding [45]. The structural behavior of HTD@GO functionalized nanocomposite is further characterized by Raman spectroscopy, as illustrated in Fig. 3b. Typically, GO Raman bands are appeared at $\sim 1356\text{ cm}^{-1}$ and $\sim 1595\text{ cm}^{-1}$ which normally refer to D band or K -point phonons of A_{1g} symmetry and Raman active G band of sp^2 hybridized carbon (the E_{2g} phonons), respectively [46, 47]. However in Fig. 3b, Raman bands for D and G in HTD@GO functionalized nanocomposites are visibly shifted from $\sim 1356\text{ cm}^{-1}$ to $\sim 1347\text{ cm}^{-1}$ and $\sim 1595\text{ cm}^{-1}$ to $\sim 1540\text{ cm}^{-1}$, favoring the interaction between HTD oligomer and GO, in particular specifying the interaction between C-S⁺ of HTD oligomer and carboxylate group of GO [50]. These results are in excellent agreement with the FTIR results.

XPS measurements are performed for HTD@GO functionalized nanocomposite to investigate the chemical states of O 1s, S 2p, and C 1s. The survey XPS

spectrum (Fig. 4a exhibits three binding energies peaks at $\sim 284.5\text{ eV}$, $\sim 164\text{ eV}$, and $\sim 520.2\text{ eV}$, representing to C 1s, S 2p, and O 1s peaks, respectively. To define the detailed structural interaction and bonding between HTD oligomer and GO, a high-resolution C 1s, S 2p, and O 1s XPS are deconvoluted. Figure 4b shows C 1s XPS spectra of HTD@GO functionalized nanocomposite with binding energies positioned at deconvoluted peaks at ~ 289.1 , ~ 286.3 , ~ 283.4 , and $\sim 284.8\text{ eV}$, referring to $^-O-C=O$, C-O, C-S, C-C, and C-H bonds [48, 49]. In Fig. 4b, the binding energy at $\sim 284.8\text{ eV}$ represents sp^2 carbon skeleton of C-C bond in GO and C-C of the benzoid ring in HTD oligomer, showing the bonding of GO-S (thiophene unit in HTD oligomer) which confirms the intermixing of C-C aromatic bond of GO and HTD oligomer. The deconvoluted O1s XPS of HTD@GO functionalized nanocomposite exhibits three binding energy peaks with one center binding energy peak, as shown in Fig. 4c.

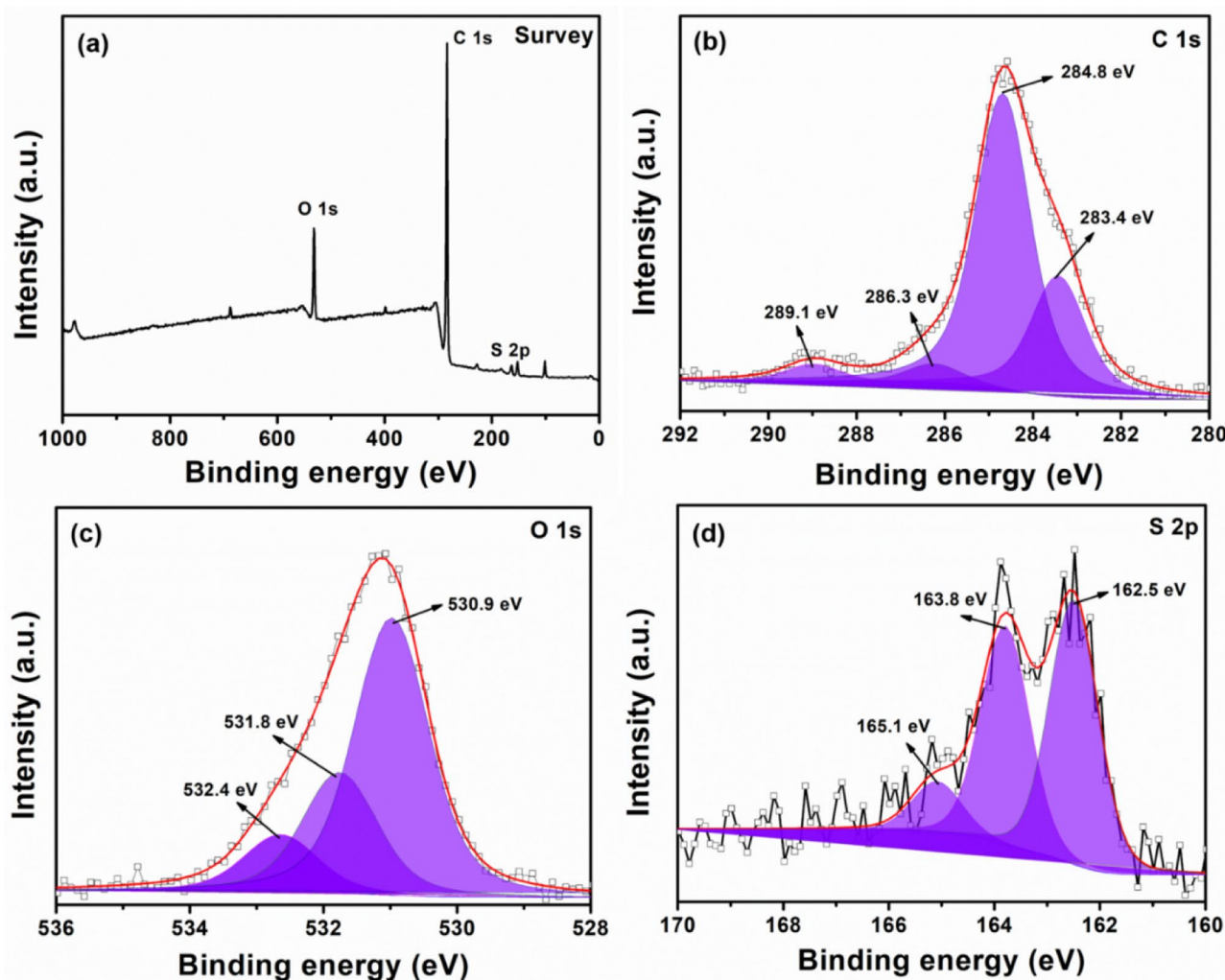


Fig. 4 a Survey, b C 1s, c O 1s, and d S 2p XPS spectra of HTD@GO functionalized nanocomposite

The binding energy positioned at ~ 530.9 eV is normally assigned to C=O or C–OH group in carbon-based materials [50]. The binding energy at ~ 531.8 eV could be attributed to C=O and O=C–O[−] functional groups in HTD@GO functionalized nanocomposite, while a higher binding energy peak at ~ 532.4 eV corresponds to the bound water molecules [51]. Figure 4d displays S 2p XPS spectrum of HTD@GO functionalized nanocomposite which is consisted of two binding energies at ~ 165.1 eV (S 2p_{1/2}) and ~ 163.8 eV (S 2p_{3/2}), resulted from C–S bond [52]. The appearance of binding energy at ~ 162.5 eV might be originated from thiophene (S) of HTD oligomer. Importantly, the position of binding energy is slightly shifted towards higher binding energy as compared to S 2p XPS of GO–S bond [53], suggesting the interaction of sulfur in HTD oligomer to carboxylate group of GO, which partially forms the hydrogen bonding.

3.4 Electrochemical characterization of HTD@GO/GCE sensor probe

3.4.1 Selectivity of metal ions detection through CV measurements

The selectivity of HTD@GO/GCE sensor probe towards heavy metal ion detection is determined by CV measurements at scan rate of 50 mV/s. Herein, the supporting electrolyte of 0.1 M PBS solution is used in different metal ion solutions of K⁺, Al³⁺, Mn²⁺, Zn²⁺, Cu²⁺, and Cr²⁺ ions. Firstly, CV plots of bare GCE, GO/GCE, and HTD@GO/GCE in 0.1 M PBS electrolyte with 0.05 M KCl are measured to explain the sensing behavior of HTD@GO functionalized nanocomposite, as shown in Fig. 5a. A weak current response is recorded with bare GCE whereas, a slightly higher response is observed for GO/GCE. Herein, a

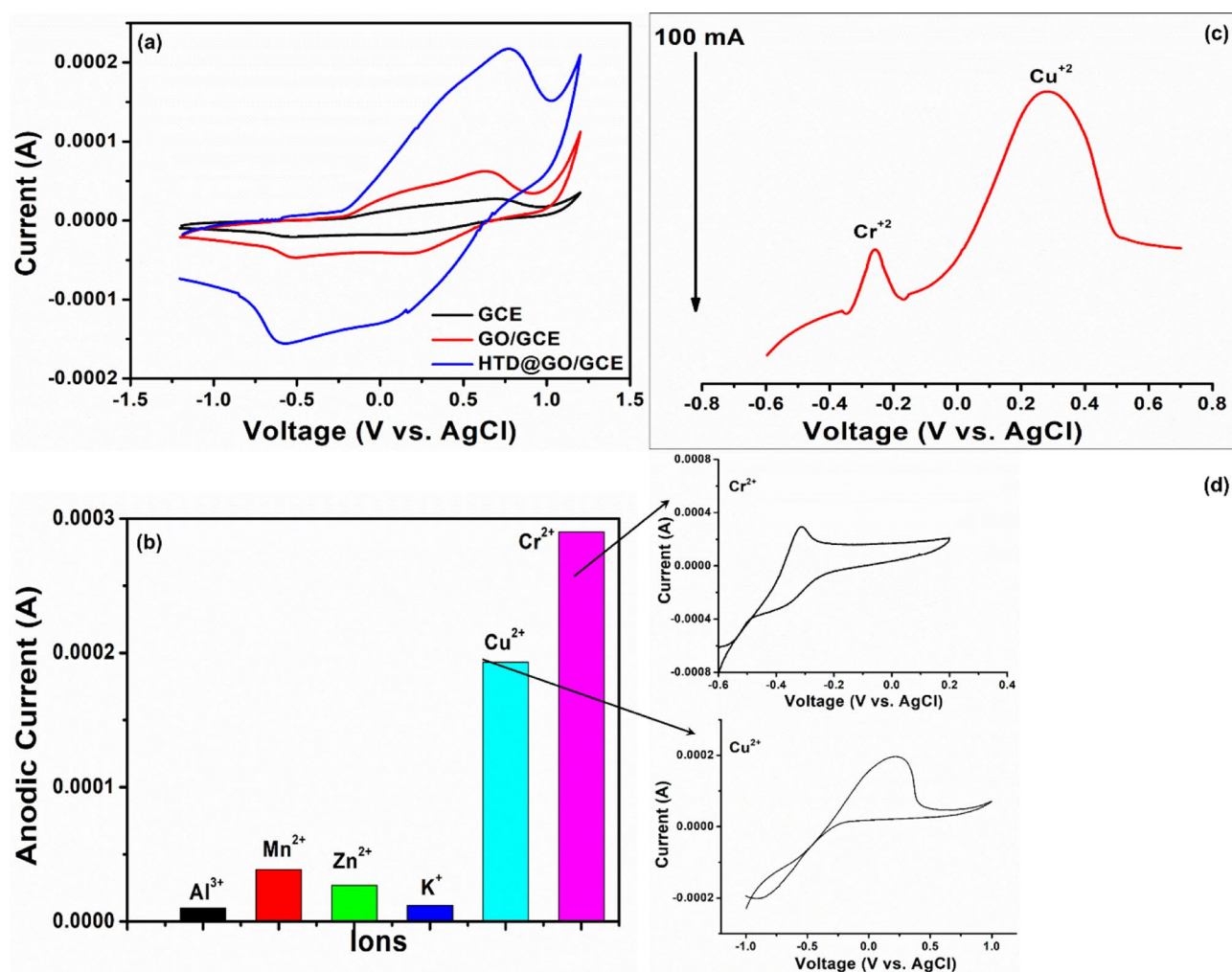


Fig. 5 **a** CV plots of bare GCE, GO/GCE, and HTD@GO/GCE sensor probe in 0.1 M PBS electrolyte; **b** CV responses using HTD@GO/GCE sensor probe towards the determination of 6 metal ions viz K⁺, Al³⁺, Mn²⁺, Zn²⁺, Cu²⁺, and Cr²⁺ ions at the uniform concen-

tration of 1 μ M; **c** simultaneous detection of Cr²⁺ and Cu²⁺ ions by SWASV using same electrode in 0.1 M PBS; and **d** CV plots of Cr²⁺ and Cu²⁺ ions measured with HTD@GO/GCE sensor probe

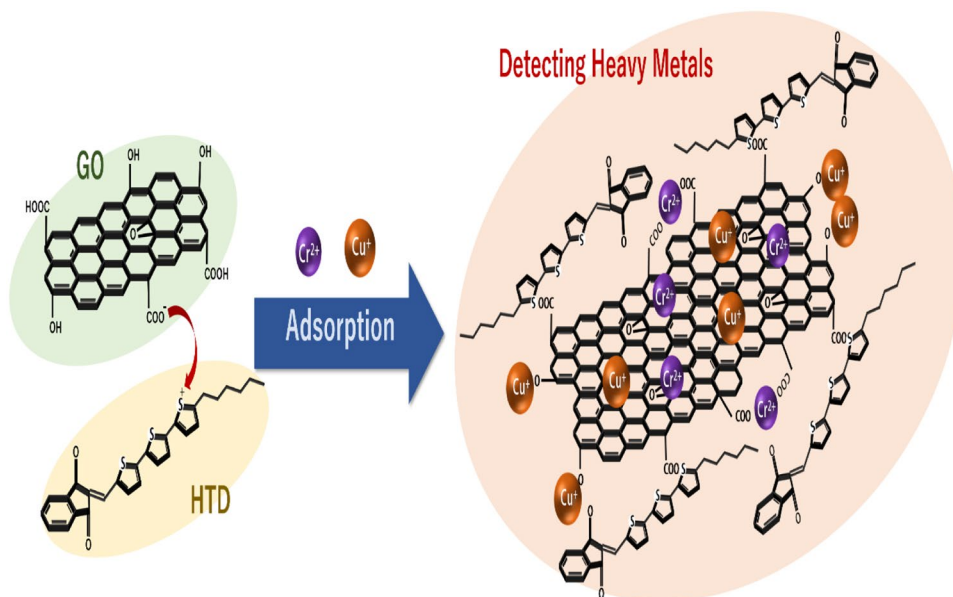
low current response in bare GCE shows the poor conductivity of GCE electrode and the slightly improved current response with GO/GCE is related to the presence of GO which has considerably increased the number of active sites over the electrode surface. As seen in Fig. 5a, a high current response for HTD@GO/GCE sensor probe is observed with the existence of significant oxidation current peak. Herein, a large specific surface area of GO, well dispersion of HTD oligomer into GO (as confirmed from FESEM results), and a good bonding between HTD oligomer and GO (corroborated from XPS results) collectively promoted the electron transfer rate and improved the surface properties of HTD@GO/GCE sensor probe. In general, the modification of GO/GCE surface with conjugated organic semiconductors is a proven strategy to improve the current response characteristics of the fabricated sensor by improving the conductivity of the electrode. In our case, the improvement of HTD@GO/GCE sensor probe is realized via a charge hopping transport mechanism of HTD oligomer through the depletion of the charge injection barrier. Figure 5b shows the CV responses using HTD@GO/GCE sensor probe towards the determination of 6 metal ions viz K^+ , Al^{3+} , Mn^{2+} , Zn^{2+} , Cu^{2+} , and Cr^{2+} ions at the concentration of $1 \mu M$. Among of all ions, a strong anodic current response for Cr^{2+} ions at $-0.31 V$ is observed, whereas Cu^{2+} ion also shows a strong anodic current response at $0.21 V$.

These responses indicate that HTD@GO/GCE sensor probe is promising for the detection of Cr^{2+} and Cu^{2+} ions in $0.1 M$ PBS electrolyte. The enhancement of the sensing signal for Cr^{2+} and Cu^{2+} ions can be ascribed to the factors of (i) HTD oligomer owns negative charges due $C-S^-$ and

$C=O^-$, causing HTD@GO/GCE sensor probe to adsorb more target ions and receive stronger signal secondly, and (ii) GO moieties provide more effective active area for the nucleation due to its large surface-to-volume ratio [54]. To further verify the feasibility of an electrochemical method for the simultaneous detection of metal ions, the presence of Cr^{2+} and Cu^+ ions is detected by stripping voltammetry using same electrode in $0.1 M$ PBS ($pH = 7$), as depicted in Fig. 5c. The peak potentials for Cr^{2+} and Cu^+ ions are observed at $\sim -0.29 V$ and $\sim -0.24 V$, respectively. Moreover, the peak intensity of Cr^{2+} ion is lower than that of Cu^{2+} peak detection intensity in the supporting electrolyte. This reduction of stripping signal might due to the formation of intermetallic compounds and the existence of competition between the analytes and the interfering ions for the active sites of HTD@GO/GCE sensor probe [55]. These results indicate that the fabricated HTD@GO/GCE sensor probe is capable of simultaneous detection of multiple heavy metal ions (such as Cr^{2+} and Cu^+ ions) with a high sensitivity.

The suggested mechanism for the determination of Cr^{2+} and Cu^+ ions is shown in Fig. 6. As described above, the combination of HTD oligomer with advantageous large surface area of GO considerably provides a large amount of active sites as well as improves the electrical conductivity of electrode, which are necessitated for high adsorption of heavy metal ions (in our case, Cr^{2+} and Cu^+ ions) and enhances the electron transfer properties of the electrode. Thus, Cr^{2+} and Cu^+ ions easily interact with the surface of HTD@GO/GCE sensor probe, resulting in increasing the current and conductance.

Fig. 6 Proposed mechanism for Cr^{2+} and Cu^+ ions detection over HTD@GO/GCE sensor probe



3.4.2 Sensitivity, reproducibility, and stability of HTD@GO/GCE sensor probe

The details of sensing properties of HTD@GO/GCE sensor probe for Cr^{2+} and Cu^{2+} ions have been further analyzed by measuring the series of CV plots using different concentrations of ions (1–100 μM) in PBS electrolyte. Figure 7a shows the CV plots of HTD@GO/GCE sensor probe for different concentrations of Cr^{2+} ions in 0.1 M PBS electrolyte. The anodic current at -0.31 V gradually increases with an increase of Cr^{2+} ions concentration, indicating an elevation in the ionic strength of an electrolyte. From Fig. 7b, a similar behavior of HTD@GO/GCE sensor probe is recorded for the detection of Cu^{2+} ions, in which an increase of Cu^{2+} ion concentration leads to the continuous enhancement in an anodic current. Thus, an anodic current in CV measurements with different ion concentration prominently explains the sensing characteristics of HTD@GO/GCE sensor probe for the determination of Cr^{2+} and Cu^{2+} ions.

Table 1 Sensing parameters of HTD@GO/GCE sensing probe for the determination of Cr^{2+} and Cu^{2+} ions

Ions	Dynamic range	LOD (μM)	R^2	Sensitivity ($\mu\text{A } \mu\text{M}^{-1} \text{cm}^{-2}$)
Cr^{2+}	1–100 μM	3.65	0.90113	483.3
Cu^{2+}	1–100 μM	2.25	0.95867	101.47

The calibration plots of anodic current responses from CV measurements for the determination of Cr^{2+} and Cu^{2+} ions are plotted in Fig. 7c, d. The sensing parameters such as sensitivity, limit of detection (LOD), linear range, and regression coefficient for the detection of Cr^{2+} and Cu^{2+} ions are summarized in Table 1. Calibration plots for Cr^{2+} and Cu^{2+} ions present a linearity of current with the increase of ion concentrations. Linear dynamic for Cr^{2+} and Cu^{2+} ions are observed as ~ 1 –100 μM , whereas reasonably good LODs of ~ 3.65 μM and ~ 2.25 μM are estimated for Cr^{2+} and Cu^{2+} ions, respectively. The results obtained by HTD@GO/GCE

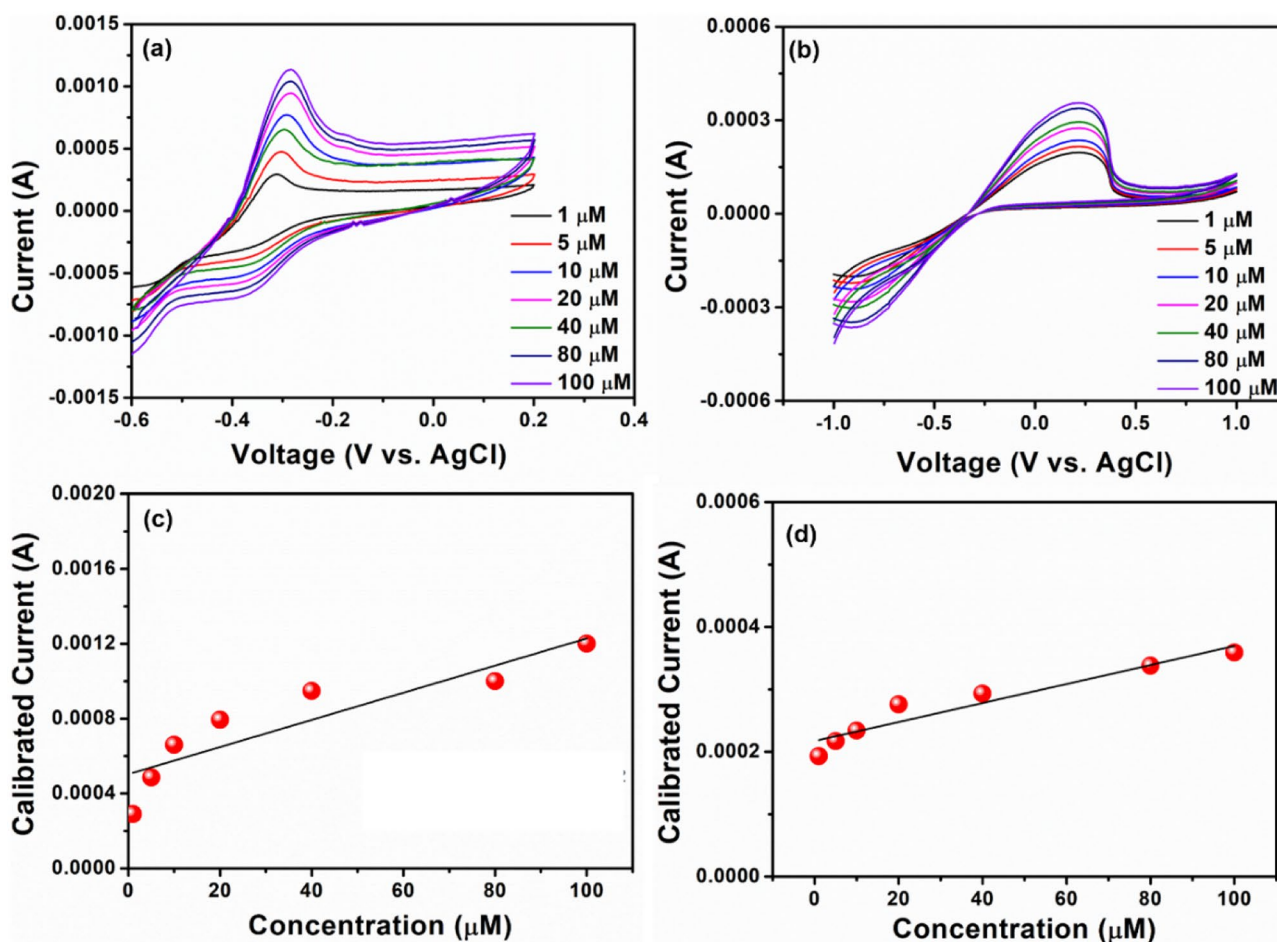


Fig. 7 CV plots of HTD@GO/GCE sensor probe for different concentrations of **a** Cr^{2+} ions and **b** Cu^{2+} ions in 0.1 M PBS electrolyte, and the calibration plot of anodic current responses from CV measurements for the determination of **c** Cr^{2+} and **d** Cu^{2+} ions

Table 2 Comparison of sensing performances with other reported chemical sensors

Electrode	Target metal	Dynamic range	LOD	<i>R</i>	Ref
4-Amino-6-hydroxy-2-mercaptopyrimidine	Cu(II)	10 pM–0.1 mM	8×10^{-9} M	0.9971	[56]
Poly(3, 4-ethylenedioxythiophene) (PEDOT)	Pb(II)	0.1 mM–0.4 M	0.19 nM	0.998	[57]
N,N-dichromone-p-phenylenediamine/ carbon paste electrode	Cu(II)	0.1–10 nM	0.096 nM	0.999	[58]
Polyaniline/glassy carbon electrode	Cd(II)	300 nM–2 μ M	130 nM	0.974	[59]
	Pb(II)	300 nM–2 μ M	100 nM	0.989	
Polyethyleneimine (PEI) decorated black phosphorus (BP) nanocomposite	Cu(II)	0.25–91 μ M	0.02 μ M	0.994	[60]
MnS/Ag-polyvinylpyrrolidone nanocomposite	Hg(II)	1–150 nM	–	16 nM	[61]
Diethyl thieno[2, 3-b]thiophene-2, 5-dicarboxylate (DETTDC2)/glassy carbon electrode	Hg(II)	0.1 nM–0.1 M	12.80 pM	0.9979	[62]
Poly(L-glutamic acid)/graphene oxide composite	Cu(II)	250 nM–5.5 μ M	24 nM	0.995	[63]
	Cd(II)		15 nM	0.982	
	Hg(II)		32 nM	0.993	
Graphene/brominated white PANi flakes	Pb(II)	0.01–0.18 μ M	0.0073 μ M	–	[64]
	Cd(II)	0.01–0.23 μM	0.0065 μ M	–	

sensor probe are compared with different electrochemical systems for the determination of metal ions, as discussed in Table 2.

The reproducibility of HTD@GO/GCE sensor probe is studied by obtaining the sensing responses from six electrodes prepared under similar conditions, as shown in

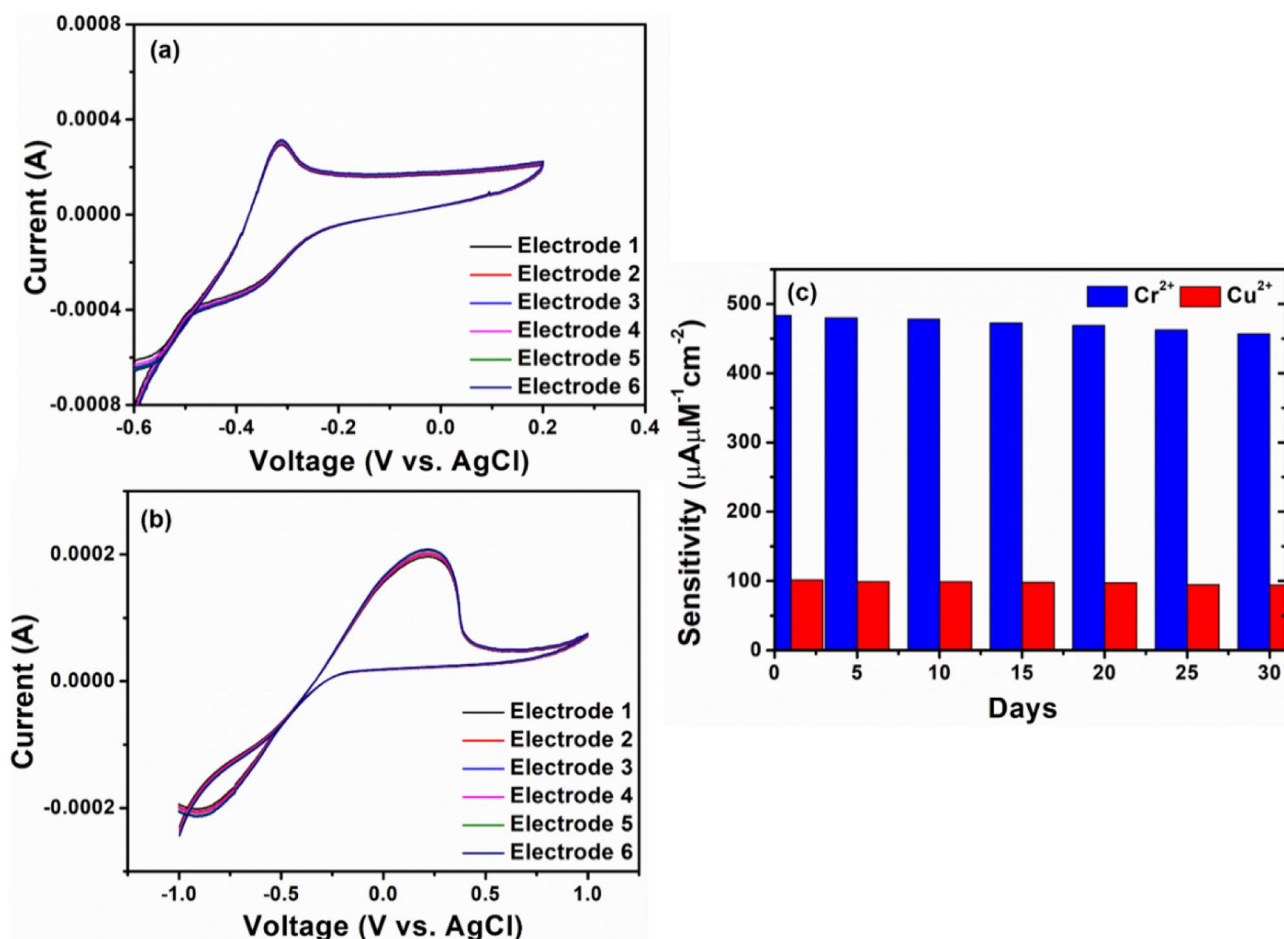


Fig. 8 Reproducibility test of HTD@GO/GCE from six electrodes for **a** Cr²⁺, **b** Cu²⁺ ions, and **c** stability test of HTD@GO/GCE sensor probe for 30 days

Fig. 8a, b. The relative standard deviations (RSDs) of Cr^{+2} and Cu^{+2} ions are calculated to be $\sim 10\%$, $\sim 6.40\%$, respectively. The obtained result indicates that HTD@GO/GCE sensor probes vary less from standard values, and therefore, this is highly reproducible and reliable sensor electrode for the detection of Cr^{+2} and Cu^{+2} ions. To explore its stability, the sensing behavior of fabricated HTD@GO/GCE sensor probe was tested for 30 days. Figure 8c presents that sensitivity of the sensor maintains the values of $\sim 92.5\%$, and $\sim 91.4\%$ for Cr^{+2} and Cu^{+2} ions, respectively, after 30 days of checking, indicating a good stability of the developed electrochemical sensor.

3.4.3 Real samples analysis of HTD@GO/GCE sensor probe

To investigate the practical applicability of the fabricated sensor with HTD@GO/GCE sensor probe, the electrochemical performance for the determination of Cr^{+2} and Cu^{+2} ions (0.1 M PBS) is checked in real sample using tap water as supporting electrolyte, as shown in Fig. 9a, b. The anodic currents of Cr^{+2} and Cu^{+2} ions are weak in bare tap water sample, indicating that the concentrations of Cr^{+2} and Cu^{+2}

ions are lower at the potentials of ~ -0.31 V, and ~ -0.21 V. Moreover, as shown in Fig. 5c, the stripping peaks exhibit well-defined and well-separated signals for Cr^{2+} and Cu^{2+} ions, indicating that the HTD@GO/GCE sensor probe can simultaneously detect the target ions at such a low concentration as 1 μM .

4 Conclusions

In this work, the planar 2-(5''-hexyl-[2,2':5'2'' terthiophen]-5-yl) methylene)-1H-indene-1,3(2H) dione oligomer (HTD) is synthesized by Suzuki-coupling reaction. Functionalized nanocomposite of HTD oligomer with graphene oxide (GO), HTD@GO, exhibits the synergic effects of HTD and GO as electrode material for the fabrication of a simple, reliable, and sensitive sensor to simultaneously detect the trace Cr^{2+} and Cu^{2+} ions. The covalently linked HTD oligomer with GO not only improves the conductivity, dispersion, and surface area of HTD@GO functionalized nanocomposite, but also supports the diffusion and promotion of the electron transfer rate. Due to unique structural characteristics and good electrochemical performance of HTD@GO functionalized nanocomposite, simultaneous detection of Cr^{2+} and Cu^{2+} ions with high sensitivity and reliability has been realized. The practicality of our fabricated sensor is validated by the recovery test of target metal ions in tap water.

Supplementary information The online version contains supplementary material available at <https://doi.org/10.1007/s42114-022-00428-z>.

Funding This research is supported by Korea Basic Science Institute under the R&D program (Project No. D010710) supervised by the Ministry of Science and ICT. This work was also supported by the national research Foundation of Korea (NRF) grant funded by the Korea government (MSIT) No-2019R1F1063999. E. B. Kim also received research grant from NRF Korea (Project No.: 2020R1A6A3A13070611). This paper was supported by the selection of research oriented professor of Jeonbuk National University in 2021. This paper is supported by the research funds of Jeonbuk National University in 2021.

Declarations

Conflict of interest The authors declare no competing interests.

References

- Kim EB, Imran M, Akhtar MS, Shin HS, Ameen S (2021) Enticing 3D peony-like ZnGa_2O_4 microstructures for electrochemical detection of N, N-dimethylmethanamide chemical. *J Hazard Mater* 404:124069
- Rahman MA, Park DS, Shim YB, Kumar P (2008) Electrochemical sensors based on organic conjugated polymers. *Sensors* 8:118–141
- Guo J, Li X, Liu H, Young DP, Song G, Song K, Zhu J, Kong J, Guo Z (2021) Tunable magnetoresistance of core-shell structured

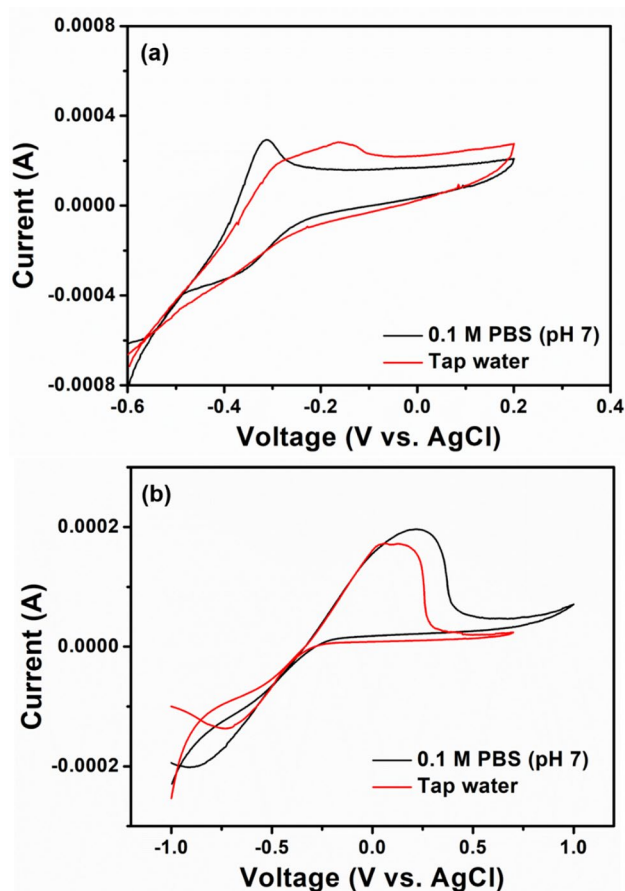


Fig. 9 Real sample applications for the determination of **a** Cr^{2+} and **b** Cu^{2+} ions

- polyaniline nanocomposites with 0-, 1-, and 2-dimensional nanocarbons. *Adv Composites Hybrid Mater* 4:51–64
4. Chen J, Zhu Y, Guo Z, Nasibulin AG (2020) Recent progress on thermo-electrical properties of conductive polymer composites and their application in temperature sensors. *Eng Sci* 12:13–22
 5. Rehman S, Ahmed R, Ma K, Xu S, Tao T, Aslam MA, Wang AM (2021) J composite of strip-shaped ZIF-67 with polypyrrole: a conductive polymer-MOF electrode system for stable and high specific capacitance. *Eng Sci* 13:11–23
 6. Elayappan V, Murugadoss V, Fei Z, Angaiah DPJ, S, (2020) Influence of polypyrrole incorporated electrospun poly(vinylidene fluoride-co-hexafluoropropylene) nanofibrous composite membrane electrolyte on the photovoltaic performance of dye sensitized solar cell. *Eng Sci* 1:78–84
 7. Guo J, Chen Z, Abdul W, Kong J, Khan MA, Young DP, Zhu J, Guo Z (2021) Tunable positive magnetoresistance of magnetic polyaniline nanocomposites. *Advan Comp Hybrid Mater* 4:534–542
 8. Guo J, Li X, Chen Z, Zhu J, Mai X, Wei R, Sun K, Liu H, Chen Y, Naik N, Guo Z (2022) Magnetic NiFe₂O₄/Polypyrrole nanocomposites with enhanced electromagnetic wave absorption. *J Mater Sci Technol* 108:64–72
 9. Park MO, Seo KD, Shim YB, Yoon JH, Park DS (2019) Chromium (VI) sensor based on catalytic reduction using the nanoporous layer of poly (aminopyrimidyl-terthiophene) and AuNi composite. *Sen Act B: Chem* 301:127151–127159
 10. Choi SM, Kim DM, Jung OS, Shim YB (2015) A disposable chronocoulometric sensor for heavy metal ions using a diamino-terthiophene-modified electrode doped with graphene oxide. *Anal Chim Acta* 892:77–84
 11. Lee WC, Kim KB, Gurudatt NG, Hussain KK, Choi CS, Park DS, Shim YB (2019) Comparison of enzymatic and non-enzymatic glucose sensors based on hierarchical Au-Ni alloy with conductive polymer. *Biosen Bioelectr* 130:48–54
 12. Srivani D, Gupta A, Bhosale SV, Puyad AL, Xiang W, Li J, Evans RA (2017) Non-fullerene acceptors based on central naphthalene diimide flanked by rhodamine or 1,3-indanedione. *Chem Comm* 53:7080–7083
 13. Razzaque S, Wang K, Hussain I, Tan B (2019) Facile synthesis of hyper crosslinked hollow microporous organic capsules for electrochemical sensing of Cu(II) ions. *Chem Eur J* 25:548–555
 14. Nordberg GF, Fowler BA, Nordberg M, Friberg L (2007) *Handbook on the toxicology of metals*, 3rd edn. Elsevier, Amsterdam
 15. Ramalingam S, Subramania A (2021) Effective removal of nitrates from the drinking water by chemical and electrochemical methods. *Eng Sci* 15:80–88
 16. Al-Zhrani S, Bedaiwi NM, El-Ramli IF, Barasheed AZ, Abduldaieem A, Al-Hadeethi Y, Umar, (2021) A underwater optical communications: a brief overview and recent developments. *Eng Sci* 16:146–186
 17. Lu YY, Liang XQ, Xu JM, Zhao ZY, Tian GM (2018) Synthesis of CuZrO₃ Nanocomposites/Graphene and their application in modified electrodes for the Co-detection of trace Pb(II) and Cd(II). *Sens Actuat B: Chem* 273:1146–1155
 18. Nidamanuri N, Li Y, Li Q, Dong M (2020) Graphene and graphene oxide-based membranes for gas separation. *Eng Sci* 9:3–16
 19. Moradi O, Madanpisheh MA, Moghaddas M (2021) Synthesis of GO/HEMA, GO/ HEMA/TiO₂, and GO/Fe₃O₄/HEMA as novel nanocomposites and their dye removal ability. *Adv Compos Hybrid Mater* 4:1185–1204
 20. Aggrwal G, Salunke-Gawali S, Gejji SP, Nikalje M, Chakravarty D, Verma PL, Gosavi-Mirkute P, Harihar S, Jadhav M, Puranik VG (2021) Reactions of 2, 3-dibromonaphthalene-1, 4-dione and pyridyl amines: X-ray structures, DFT investigations, and selective detection of the Hg²⁺ and Ni²⁺ Ions. *Eng Sci* 14:78–93
 21. Hamilton MA, Rode PW, Merchant ME, Sneddon J (2008) Determination and comparison of heavy metals in selected seafood, water, vegetation and sediments by inductively coupled plasma-optical emission spectrometry from an industrialized and pristine waterway in Southwest Louisiana. *Micro Chem J* 88:52–55
 22. Sen I, Shandil A, Shrivastava VS (2011) Study for determination of heavy metals in fish species of the River Yamuna (Delhi) by inductively coupled plasma-optical emission spectroscopy (ICP-OES). *Adv In App Sci Res* 2:161–166
 23. Pizarro J, Segura R, Tapi D, Navarr F, Fuenzalid F, Aguirre MJ (2020) Inexpensive and green electrochemical sensor for the determination of Cd (II) and Pb (II) by square wave anodic stripping voltammetry in bivalve mollusks. *Food Chem* 321:126682
 24. Lu M, Deng Y, Luo Y, Lv J, Li T, Xu J, Chen SW, Wang J (2019) Graphene aerogelmetal-organic framework-based electrochemical method for simultaneous detection of multiple heavy-metal ions. *Anal Chem* 91:888–895
 25. Pooja S, Lajju RK, Utkarsh C, Chandrakala CB (2021) Face detection using deep learning to ensure a coercion resistant blockchain-based electronic voting. *Eng Sci* 16:341–353
 26. Hong J, Kang L, Shi X, Wei R, Mai X, Pan D, Naik N, Guo Z (2022) Highly efficient removal of trace lead (II) from wastewater by 1,4-dicarboxybenzene modified Fe/Co metal organic nanosheets. *J Mater Sci Technol* 98:212–218
 27. Adraoui I, Rhazi ME, Amine A, Idrissi L, Curulli A, Palleschi G (2005) Modulation of electrical properties in single-walled carbon nanotube/conducting polymer composites. *Electroanalysis* 17:685–693
 28. Renaudin SG, Moreau M, Despas C, Meyer M, Denat F, Lebeau B, Walcarius A (2009) Voltammetric detection of Pb (II) using amide-cyclam-functionalized silica-modified carbon paste electrodes. *Electroanalysis* 21:1731–1742
 29. Armstrong KC, Tatum CE, Chambers RND, Sparks JQ, Xue ZL (2010) Individual and simultaneous determination of lead, cadmium, and zinc by anodic stripping voltammetry at a bismuth bulk electrode. *Talanta* 82:675–680
 30. Wang X, Qi Y, Shen Y, Yuan Y, Zhang L, Zhang C, Sun Y (2020) A ratiometric electrochemical sensor for simultaneous detection of multiple heavy metal ions based on ferrocene-functionalized metal-organic framework. *Sen Actuat B: Chem* 310:127756–127769
 31. Xu Z, Liu Z, Xiao M, Jiang L, Yi C (2020) A smartphone-based quantitative point-of-care testing (POCT) system for simultaneous detection of multiple heavy metal ions. *Chem Eng J* 394:124966–124975
 32. Suvina V, Krishna SM, Nagaraju DH, Melo JS, Balakrishna RG (2018) Polypyrrole-reduced graphene oxide nanocomposite hydrogels: a promising electrode material for the simultaneous detection of multiple heavy metal ions. *Mater Lett* 232:209–212
 33. Peng QM, Guo JX, Zhang QR, Xiang JY, Liu BZ, Zhou AG, Liu RP, Tian YJ (2014) Unique lead adsorption behavior of activated hydroxyl group in two dimensional titanium carbide. *J Am Chem Soc* 136:4113–4116
 34. Deng W, Tan Y, Fang Z, Xie Q, Li Y, Liang X, Yao S (2009) ABTS-multiwalled carbon nanotubes nanocomposite/Bi film electrode for sensitive determination of Cd and Pb by differential pulse stripping voltammetry. *Electroanalysis* 21:2477–2485
 35. Zhang DC, Zhang X, Chen Y, Yu P, Wang CH, Ma YW (2011) Enhanced capacitance and rate capability of graphene/polypyrrole composite as electrode material for supercapacitors. *J Power Sour* 196:5990–5996
 36. Alam S, Akhtar MS, Abdullah KEB, Shin HS, Ameen S (2020) New energetic indandione based planar donor for stable and efficient organic solar cells. *Sol Energy* 201:649–657

37. Ameen S, Akhtar MS, Seo HK, Shin HS (2014) ZnO quantum dots engrafted graphene oxide thin film electrode for low level detection of ethylacetate. *Mater Lett* 136:379–383
38. Xu YX, Bai H, Lu GW, Li C, Shi GQ (2008) Chemically converted graphene induced molecular flattening of 5,10,15,20-tetrakis(1-methyl-4-pyridinio) porphyrin and its application for optical detection of cadmium (II) ions. *J Am Chem Soc* 130:5856–5857
39. Gupta V, Lai LF, Datt R, Chand S, Heeger AJ, Bazan GC, Singh SP (2016) Dithienogermole-based solution-processed molecular solar cells with efficiency over 9 %. *Chem Comm* 52:8596–8599
40. Venugopal GD, Krishnamoorthy K, Mohan R, Kim SJ (2012) An investigation of the electrical transport properties of graphene-oxide thin films. *Mat Chem Phys* 132:29–33
41. Wang H, Hao Q, Yang X, Lu L, Wang X (2010) Effect of graphene oxide on the properties of its composite with polyaniline. *ACS Appl Mater Inter* 2:821–828
42. Revoju S, Biswas S, Eliasson B, Sharma GD (2018) Effect of acceptor strength on optical, electrochemical and photovoltaic properties of phenothiazine-based small molecule for bulk heterojunction organic solar cells. *Dyes Pigm* 149:830–842
43. Perjéssy A, Hrnčiar P (1971) The C=O stretching bands of 1,3-indandione derivatives. *Tetrahedron* 27:6159–6169
44. Kaneti J, Yuchnovski I (1970) Electronic substituent effects and carbonyl stretching frequencies of 2-arylmethylene-1, 3-indandiones. *Tetrahedron* 26:4397–4402
45. Bera M, Chandravati GP, Maji PK (2018) Facile one-pot synthesis of graphene oxide by sonication assisted mechanochemical approach and its surface chemistry. *J Nanosci Nanotech* 18:902–912
46. Ferrari AC, Robertson J (2000) Interpretation of Raman spectra of disordered and amorphous carbon. *Phys Rev B* 61:14095–14107
47. Cancado LG, Pimenta MA, Neves BRA, Dantas MSS, Jorio A (2004) Influence of the atomic structure on the Raman spectra of graphite edges. *Phys Rev Lett* 93:247401–247405
48. Ameen S, Akhtar MS, Shin HS (2012) Hydrazine chemical sensing by modified electrode based on in situ electrochemically synthesized polyaniline/graphene composite thin film. *Sens Actuat B: Chem* 173:177–183
49. Tang L, Wang Y, Li Y, Feng H, Lu J, Li J (2009) Preparation, structure, and electrochemical properties of reduced graphene sheet films. *Adv Funct Mater* 19:2782–2789
50. Akhavan O (2010) The effect of heat treatment on formation of graphene thin films from graphene oxide. *Carbon* 48:509–519
51. Yang D, Velamakanni A, Bozoklu G, Park S, Stoller M, Piner RD, Stankovich S, Jung I, Field DA, Ventrice CA, Ruoff RS (2009) Chemical analysis of graphene oxide films after heat and chemical treatments by X-ray photoelectron and micro-Raman spectroscopy. *Carbon* 47:145–152
52. Ye J, He F, Nie J, Cao Y, Yang H, Ai X (2015) Sulfur/carbon nanocomposite-filled polyacrylonitrile nanofibers as a long life and high capacity cathode for lithium-sulfur batteries. *J Mater Chem A* 3:7406–7412
53. Wang X, Gao T, Han F, Ma Z, Zhang Z, Li J, Wang C (2016) Stabilizing high sulfur loading Li–S batteries by chemisorption of polysulfide on three-dimensional current collector. *Nano Ener* 30:700–708
54. Lee EJH, Zhi LJ, Burghard M, Mullen K, Kern K (2010) Electrical properties and photoconductivity of stacked-graphene carbon nanotubes. *Adv Mat* 22:1854–1857
55. Pizarro J, Segura R, Tapia D, Navarro F, Fuenzalida F, Aguirre MJ (2020) Inexpensive and green electrochemical sensor for the determination of Cd (II) and Pb (II) by square wave anodic stripping voltammetry in bivalve mollusks. *Food Chem* 321:126682
56. Oztekin Y, Ramanaviciene A, Ramanavicius A (2011) Electrochemical copper (II) sensor based on self-assembled 4-amino-6-hydroxy-2-mercaptopyrimidine monohydrate. *Sens Actuat B Chem* 155:612–617
57. Yasri NG, Halabi AJ, Istamboulie G, Nogue T (2011) Chronoamperometric determination of lead ions using PEDOT:PSS modified carbon electrodes. *Talanta* 85:2528–2533
58. Traore D, Abdelaziz ASM, Brou YS, Trokourey A (2014) Determination of Cu²⁺ by N, N-dichromone-p-phenylenediamine modified carbon paste electrode. *Int J Biol Chem Sci* 8:2773–2785
59. Wang Z, Liu E, Zhao X (2011) Glassy carbon electrode modified by conductive polyaniline coating for determination of trace lead and cadmium ions in acetate buffer solution. *Thin Solid Films* 519:5285–5289
60. Li Y, Shi Z, Zhang C, Wu X, Liu L, Guo C, Li CM (2021) Highly stable branched cationic polymer-functionalized black phosphorus electrochemical sensor for fast and direct ultratrace detection of copper ion. *J Colloid Interf Sci* 603:131–140
61. Syed A, Marraiki N, Al-Rashed S, Elgorban AM, Yassin MT (2021) A potent multifunctional MnS/Ag-polyvinylpyrrolidone nanocomposite for enhanced detection of Hg²⁺ from aqueous samples and its photocatalytic and antibacterial applications. *Spectrochim Acta Mol Biomol Spectrosc* 244:118844
62. Rahman MM, Alamry KA, Awual MR, Mekky AEM (2020) Efficient Hg(II) ionic probe development based on one-step synthesized diethyl thieno[2, 3-b]thiophene-2, 5-dicarboxylate (DETTDC2) onto glassy carbon electrode. *Microchem J* 152:104291
63. Yi W, He Z, Fei J, He X (2019) Sensitive electrochemical sensor based on poly(L-glutamic acid)/graphene oxide composite material for simultaneous detection of heavy metal ions. *RSC Adv* 9:17325–17334
64. Hashemi SA, Bahrani S, Mousavi SM, Omidifar N, Arjmand M, Lankarani KB, Ramakrishna S (2022) Simultaneous electrochemical detection of Cd and Pb in aquatic samples via coupled graphene with brominated white polyaniline flakes. *Euro Polym J* 162:110926

Publisher's Note Springer Nature remains neutral with regard to jurisdictional claims in published maps and institutional affiliations.